ACS APPLIED MATERIALS & INTERFACES

Research Article

www.acsami.org

Influence of Temperature on Oxidation Mechanisms of Fiber-Textured AlTiTaN Coatings

Vishal Khetan,[†,§] Nathalie Valle,[†] David Duday,*[,†] Claude Michotte,[‡] Marie-Paule Delplancke-Ogletree,[§] and Patrick Choquet[†]

[†]Centre de Recherche Public-Gabriel Lippmann, Science and Analysis of Materials Department, Belvaux L-4422, Luxembourg

[‡]Ceratizit Luxembourg S.à.r.l., Route de Holzem, B.P. 51, L-8201 Mamer, Luxembourg

[§]Université Libre de Bruxelles CP165/63, avenue F. D. Roosevelt 50, 1050 Bruxelles, Belgium

ABSTRACT: The oxidation kinetics of AlTiTaN hard coatings deposited at 265 °C by DC magnetron sputtering were investigated between 700 and 950 °C for various durations. By combining dynamic secondary ion mass spectrometry (D-SIMS), X-ray diffraction (XRD), and transmission electron microscopy (TEM) investigations of the different oxidized coatings, we were able to highlight the oxidation mechanisms involved. The TEM cross-section observations combined with XRD analysis show that a single amorphous oxide layer comprising Ti, Al, and Ta formed at 700 °C. Above 750 °C, the oxide scale transforms into a bilayer oxide comprising an Al-rich upper oxide layer and a Ti/Ta-rich oxide layer at the interface with the coated nitride layer. From the D-SIMS analysis, it could be proposed that the oxidation mechanism was governed primarily by inward diffusion of O for temperatures of ≤700 °C, while at ≥750 °C, it is controlled by outward diffusion of Al and inward diffusion of O. Via a combination of structural and chemical analysis, it is possible to propose that crystallization of rutile lattice favors the outward diffusion of Al within the AlTiTa mixed oxide layer with an increase in the temperature of oxidation. The difference in the mechanisms of oxidation at 700 and 900 °C also influences the oxidation kinetics with respect to oxidation time. Formation of a protective alumina layer decreases the rate of oxidation at 900 °C for long durations of oxidation compared to 700 °C. Along with the oxidation behavior, the enhanced thermal stability of AlTiTaN compared to that of the TiAlN coating is illustrated.

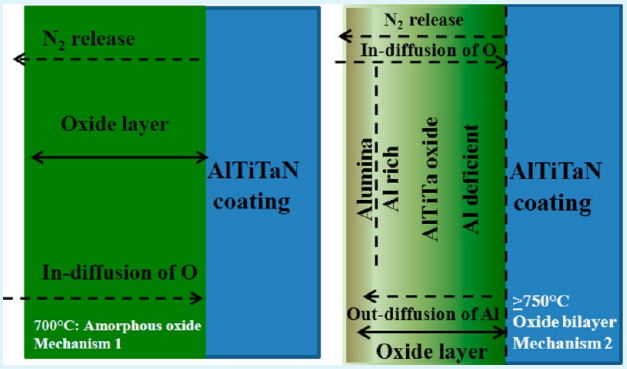

KEYWORDS: *TiAlTaN, hard coatings, fiber texture, oxidation, D-SIMS, STEM, HAADF, mechanism*

1. INTRODUCTION

Hard nanostructured TiAlN coatings have become important in the field of wear and oxidation resistant coatings.[1,2] Nevertheless, their use in high-temperature (>800 °C) applications such as dry high-speed machining remains a challenging issue. Additional alloying elements such as Si and Ta have been shown to have a beneficial impact on their high-temperature properties.[3−8] It is well-known that Al in a solid solution formed with TiN provides additional oxidation resistance at high temperatures (≤900 °C) by forming a protective alumina layer on top of the coating by means of outward diffusion of Al through the coating.[2] The presence of Ti within the coating provides the necessary hardness and toughness to the coating but also leads to formation of TiO_2, which generates stress between the oxide−nitride interfaces due to the difference in molar volume between the two as described by McIntyre et al.[2] Hence, this affects the adhesion of alumina to the coating. Also, the low activation energy for diffusion of O within TiO_2 promotes the further oxidation of Ti present within the coating. Additionally, Ta when added to TiAlN plays a significant role in improving the oxidation resistance of the coating.[6] It has been suggested in the literature that the replacement of Ti^{4+} with Ta^{5+} in TiO_2 formed at an elevated temperature (≥800 °C) reduces the oxygen vacancies, which limits the inward diffusion of oxygen in the coating and provides better oxidation resistance.[6] This in turn aids in decreasing the extent of further TiO_2 formation. For further improvements of the properties of these coatings, e.g., by addition of a fourth metallic element, a better understanding of the oxidation mechanisms over a wider range of temperature is needed.

Researchers have investigated the oxidation kinetics of TiAlN coatings over the past two decades. McIntyre et al.[2] and Ichimura et al.[9] independently studied oxidation mechanisms occurring in TiN and TiAlN coatings over the temperature range from 750 to 900 °C. Both of them showed that inward diffusion of oxygen and outward diffusion of Al are processes controlling the mechanism of oxidation within this temperature range. McIntyre et al. confirmed this process using iridium marker experiments. Later, Joshi et al.[10] also investigated the oxidation behavior of

Received: December 12, 2013
Accepted: February 18, 2014
Published: February 18, 2014

   dx.doi.org/10.1021/am405727p | ACS Appl. Mater. Interfaces 2014, 6, 4115−4125

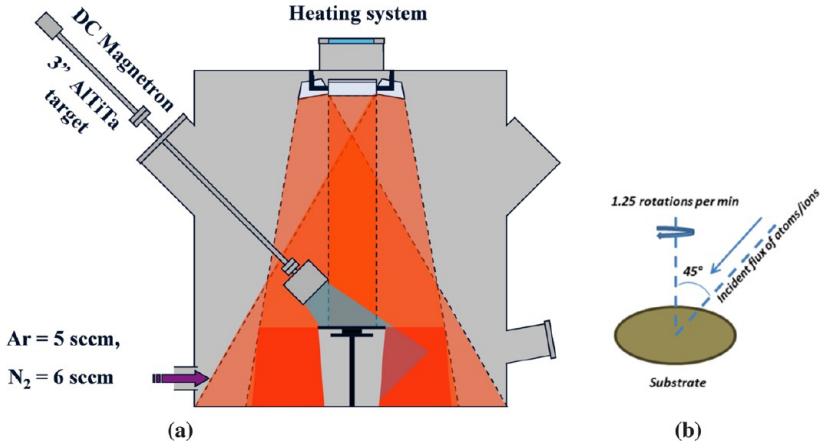

Figure 1. (a) DC magnetron sputtering system and (b) deposition angle and substrate rotation.

TiAlN over a wider temperature range (600−877 °C) and highlighted the existence of two different oxidation mechanisms prevailing during oxidation of these coatings by focusing on oxidation chemistry. They demonstrated via Auger electron spectroscopy depth profiles that inward diffusion of oxygen controlled the oxidation at <700 °C while both inward diffusion of O and outward diffusion of Al controlled the oxidation process at ≥800 °C.

In addition, Pfeiler et al.[6] and Rachbauer et al.[8] independently demonstrated the AlTiTaN coatings have better oxidation resistance than TiAlN coatings within the temperature range of 800−950 °C when deposited using cathodic arc evaporation and magnetron sputtering, respectively. Nevertheless, a clear correlation between the structure of the oxide formed and the oxidation mechanism in TiAlN or TiAlTaN coatings has not been investigated.

Looking at the potential of AlTiTaN coatings as excellent oxidation resistant coatings,[6−8] this work focuses on the oxidation mechanism of this coating. The study provides an understanding of the oxidation mechanisms involved in AlTiTaN coatings in terms of structure, microstructure, and oxidation chemistry evolution as a function of temperature. Also, this work demonstrates that coatings deposited using DC magnetron sputtering at a low deposition temperature (265 °C) provide hardness and oxidation resistance comparable to those reported in the state-of-the-art coating[6−8] at ≤950 °C. This study includes the kinetics of the reaction supporting the oxidation mechanisms involved.

2. EXPERIMENTAL SECTION

2.1. Coating Deposition. $Al_{0.48}Ti_{0.40}Ta_{0.12}N$ films were deposited in an in-house DC magnetron sputtering system. A 3 in. $Al_{46}Ti_{42}Ta_{12}$ target placed at an angle of 45° with respect to the substrate holder and at a distance of 9 cm (Figure 1) was used. The chamber was first pumped down to typically 3×10^{-7} mbar and preheated at 265 °C, and then 5 sccm of argon and 6 sccm of N_2 were injected, yielding a working pressure of 0.5 Pa. These flows were determined via a target poisoning study to allow sputtering in compound mode.

Prior to deposition, the target was presputtered at a deposition power of 300 W (power density of 6.6 W/cm^2 and target voltage of 385 V) for 10 min before deposition to decrease the amount of contaminants (e.g., O) in the coatings. To ensure a uniform thickness of the coating, the substrate was rotated in the horizontal plane at 1.25 rpm. The substrates used for oxidation tests were 20 mm × 7 mm × 0.50 mm pieces of Si (100) wafers. The bias voltage was kept constant at −100 V. The thicknesses and deposition rates of the coatings were in the range of 2.5−3.0 μm and 0.8−1.0 μm/h, respectively.

2.2. Characterization. The chemical composition of the coatings was determined by combining energy dispersive X-ray spectroscopy (EDX) and wavelength dispersive X-ray spectroscopy (WDX), using a Hitachi SU 70 scanning electron microscope with an accelerating voltage of 20 keV. The relative content in Ta was measured by WDX (error of 0.5 atom %), whereas relative contents in Ti, Al, N, and O were determined by EDX (error of 1.0 atom %). The cross-section scanning electron microscopy (SEM) imaging of the samples was performed in high-resolution mode with an accelerating voltage of 5 keV. Thickness measurements were taken in a Tencor P-10 surface profilometer. This profilometer was also used to evaluate macroscopic stress in the coating using the wafer curvature method.[11] Crystallographic investigations of as-deposited coatings were performed in the $\theta - 2\theta$ Bragg−Brentano (BB) configuration in a Bruker D8 discover diffractometer using Cu Kα radiation. Glancing incidence (GI) XRD measurements were performed for phase identification of as-deposited and oxidized samples at a glancing angle of 2°. The stress in the coating was evaluated using the $\sin^2 \psi$ method with XRD technique. Elastic constants considered for measurement were for a TiAlN coating, and their values are as follows: Young's modulus of 450 MPa and Poisson's coefficient of 0.177. Oxidation of the coatings in air was performed in the X-ray diffractometer, using its *in situ* heating capability. An Anton Paar TCU 200 temperature control unit was used as the *in situ* heating system. Oxidation temperatures ranging from 700 to 950 °C were applied, for various durations (from 1 min to 15 h). The conditions of oxidation are summarized in Table 1. The heating and cooling rate was set to 1 °C/s.

Table 1. List of Oxidation Experiments Performed

	700 °C	750 °C	800 °C	850 °C	900 °C	950 °C
1 min	na[a]	na[a]	na[a]	na[a]	×	na[a]
1 h	×	×	×	×	×	×
2 h	na[a]	na[a]	na[a]	na[a]	×	na[a]
6 h	×	na[a]	na[a]	na[a]	×	na[a]
15 h	×	na[a]	na[a]	na[a]	na[a]	na[a]

[a]Not applicable.

After oxidation, the samples were cooled to room temperature using air flow in the XRD heating system. Hardness measurements were taken in a nanoindentation tester using a Berkovich indenter at CSM instruments (Peseux, Switzerland). Chemical depth profiling was conducted via secondary ion mass spectrometry (SIMS) in a CAMECA SC-Ultra instrument in positive ion mode, using Cs^+ ions with an impact energy of 1.0 or 3.5 keV, depending on the thickness of the oxide analyzed. The typical acquisition time for the D-SIMS profiles ranged from 1 to 3 h depending on the thickness of the oxide developed and the energy of Cs^+ ions used. The thicknesses of total oxide layers were determined by combining the D-SIMS and surface profilometry techniques. In a few cases, they were also determined using SEM and

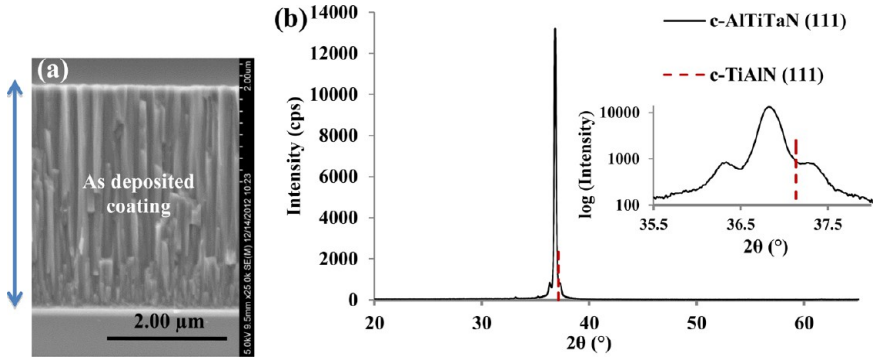

Figure 2. (a) SEM cross-section image and (b) $\theta - 2\theta$ XRD pattern of an as-deposited $Al_{0.48}Ti_{0.40}Ta_{0.12}N$ coating (the inset shows XRD spectra on a semilogarithmic scale). The vertical line indicates the standard position of the cubic TiAlN structure corresponding to JCPDS File 04-005-5251 [TiAlN (111), 37.13].

transmission electron microscopy (TEM) techniques. The values obtained from these three techniques were in good agreement. The evolution of the thickness of the aluminum oxide layer with oxidation time could be determined by comparing the sputtering times necessary to sputter the different whole aluminum oxide layers (provided the SIMS analytical conditions were similar). A FEI Helios Nanolab 650 dual beam (scanning electron microscope equipped with a focused ion beam) was used to prepare the 900 °C oxidized sample for TEM characterization. TEM investigations (imaging, composition, and electron diffraction) were performed in a LEO 922 OMEGA instrument operating at 200 kV. A high-angle annular dark field (HAADF) image was obtained on a Libra200 Cs-STEM instrument at the center of advanced European studies and research (CAESAR) in Bonn, Germany.

3. RESULTS

3.1. Texture and Stress of As-Deposited Coatings. The relative elemental contents for the as-deposited coatings were 23 atom % Al, 20 atom % Ti, 6 atom % Ta, 48 atom % N, and 3 atom % O. The Ta content was selected on the basis of results reported by Rachbauer et al.,[8] in the range of 3−10 atom % Ta to ensure good thermal stability for AlTiTaN coatings. Furthermore, 6 atom % Ta was shown by Sangiovanni et al.[12] to yield maximal toughness.

The SEM cross-section image (Figure 2a) shows the development of columnar structure in the as-deposited coating. A dense fine-grain structure corresponding to zone T of Thornton's structure zone model[13] could be observed.

The $\theta - 2\theta$ XRD measurements for the coating can be seen in Figure 2b. The coating exhibits a single-phase cubic structure with a (111) preferred crystallographic orientation, and the presence of satellites on both sides of the (111) peak can also be reported. The presence of these satellites could be correlated with a coating with a periodic variation of the coating density along the thickness, something similar to the observation of a multilayer structure. The deposition chamber geometry (sputtering source positioned opposite, 45° from substrate normal) and the sample holder operating speed (7.5 °C/s) are likely to induce a periodic modulation of the coating composition, generating a multilayer structure through the thickness. This composition modulation is consistent with the exclusive observation of the first-order {111} satellite peaks because it necessarily involves progressive composition evolution and thus diffuse interfaces. According to the method of Fullerton et al.,[14] the periodicity of bilayers can be calculated from the position of the satellites on the XRD spectrum. The periodicity extracted from satellite XRD peak positions (16.7 ± 0.2 nm) is similar to that obtained by dividing the coating thickness by the number of stage revolutions (15 ± 2 nm), confirming the origin of these peaks. The stress in the coatings was determined to be −0.07 ± 0.01 and 0.42 ± 0.05 GPa using the wafer curvature method and XRD ($\sin^2 \psi$ technique), respectively.

This result differs from those of Rachbauer et al.,[8] with similar Ta content in TiAlN coatings where both (111) and (200) crystallographic orientations coexist but were deposited under deposition conditions (higher deposition temperature and different bias voltage) different from those used in this work. The lattice parameter was determined to be 4.2277 Å using XRD data and was higher than 4.1899 Å, which is the lattice parameter corresponding to the standard c-TiAlN (111) phase. Because the stress level is low, the peak position is mainly related to an alloying effect, the shift to lower angles being explained by the addition of Ta. More recently, Abadias et al.[15] observed a correlation between the stress and the development of a preferred orientation in TiN coatings. Coatings with tensile or zero stress primarily develop a (111) texture due to attractive forces at the grain boundary and/or void formation, while "atomic peening" (incorporation of point defects in the film induced by the bombardment of energetic species) favors a (200) preferred orientation. In our case, these low values of stress can be explained by a relatively high working pressure (0.5 Pa) that reduces the contribution of ion bombardment (atomic peening), because 265 °C is a relatively low substrate temperature for such nitride coatings, and/or by the low deposition rate (0.25 nm/s), which favor structures with lower concentrations of defects and low residual stress. The multilayer structure, which can relax stresses at interfaces, can also play a role in the minimization of stress.

3.2. Mechanical Properties of As-Deposited Coatings. The hardness of the coating was measured to be 33 ± 2 GPa, and the elastic modulus was determined to be 415 ± 30 GPa, resulting in a hardness/elastic modulus ratio of 0.08. This hardness is below that reported by Rachbauer et al.[8] (~42 GPa) for a similar Ta concentration (5 atom %), but in their case, the coatings exhibited higher compressive stresses and a (200) preferred orientation because of a substrate temperature of 500 °C, a faster deposition rate, a shorter target−sample distance, and a lower pressure. The value is in agreement with the value of 30 GPa predicted by Sangiovanni et al.[12] through density functional theory calculations for a 6 atom % Ta alloyed TiAlN.

3.3. Oxidation Study between 700 and 950 °C. The evolution with time of the oxide thicknesses of the coated samples during the oxidation tests between 700 and 950 °C was measured. Only the values for 700 and 900 °C are reported in Figure 3. From these results, it can be considered that oxidation

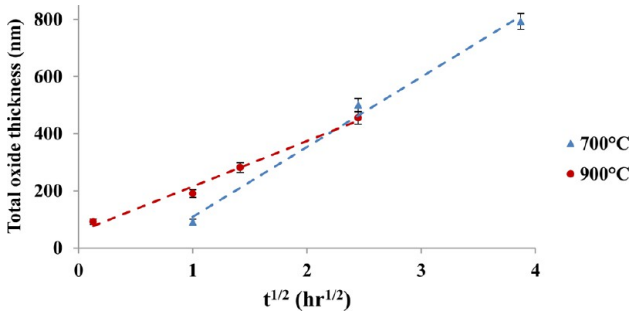

Figure 3. Variation of the oxide thickness with the square root of time at 700 and 900 °C.

mechanisms are controlled by parabolic law with a rate constant depending of the oxidation temperature. This indicates a protective behavior with a growing diffusion barrier effect with time in both cases. By evaluating the oxide layer thickness versus the square root of time, we can report that the evolution is linear for both temperatures and that the rate constants of the oxide layer thickness at 700 and 900 °C were found to be 16.8 ± 0.2 and 7.3 ± 0.1 nm^2/s, respectively. Thus, at 900 °C, the level of protection provided by coatings is higher. Quantitatively, this was further verified by the thickness of oxides measured. These total oxide layer thicknesses were 500 ± 22 and 455 ± 20 nm at 700 and 900 °C respectively. At 700 °C, the oxidation rate is too slow to determine the oxide thickness after 1 min. Therefore, in Figure 3, the oxide thickness is determined for a 1 h oxidation.

To improve our understanding of the oxide growth mechanism, oxidized coatings were investigated by XRD. The $\theta - 2\theta$ measurements performed on the air-annealed samples show a high angle shift for the peak corresponding to the AlTiTaN cubic (111) phase (from 36.8° to 37.1°) at all the temperatures tested, as well as the disappearance of the satellite peaks, perhaps because of the disappearance of the multilayer structure with an increase in atom mobility (Figure 4a). The shift is toward the fcc TiNO (111) peak at 37.05°. A similar peak shift to high angles and a peak broadening were also observed after annealing at a low pressure (10^{-3} mbar) with an increase in the full width at half-maximum from 0.22 to 0.78. Both peak broadening and peak shift can be explained by the incorporation of oxygen at the grain boundary and inside grains, which increases microstrain and degrades crystallinity as oxidation was conducted in air at ≤850 °C, and although a possible decomposition of TiAlTaN cannot be completely ignored at ≤850 °C, the possibility of such decomposition is minimal due to the fact that Ta acts as a strengthening element for TiAlN coatings at these temperatures as demonstrated by Holec et al.[16] In addition, the broad peak observed at 37.1° postoxidation could not be attributed to any specific phase except for fcc (AlTa)TiNO (111). A more important shift, from 62.05° to 62.75°, is also observed for the AlTiTaN (220) reflections in the GI XRD patterns (Figure 6b) displaying a similar observation.

The structure of the oxide scales of the air annealed samples was also investigated by GI XRD. The XRD patterns of the samples oxidized for 1 h in air at temperatures ranging from 700 to 950 °C are shown in Figure 4b. At 700 °C, the absence of reflections other than the (220) of fcc AlTiTaN suggests that the oxides could be amorphous. At this temperature, even after a relatively long oxidation exposition, 15 h, no crystallization was observed (XRD spectra not presented here). At 750 °C, a small (101) rutile peak appears and its intensity increases as the temperature increases (keeping the duration constant), suggesting that the crystallization of the Ti oxide becomes more important between 800 and 950 °C, with the appearance of a second rutile (211) peak at 800 °C. No significant change in intensity was observed for the peak corresponding to the (211) plane. Only the reflections corresponding to (101) and (211) planes in rutile were observed, with a slight shift toward lower angles. No evidence of any Ta- or Al-based oxide could be detected. Guidi et al.[17] showed that Ta^{5+} can substitute for Ti^{4+} in the rutile lattice because of their similar ionic radii (0.61 Å for Ti^{4+} and 0.65 Å for Ta^{5+}), which could account for the absence of a crystalline Ta-based oxide. Similar arguments have been used by Pfeiler et al.[6] and Reddy et al.[18] to explain the absence of tantalum oxide on their XRD spectra. No alumina peak reflections have been detected for these different oxidized samples.

The GI XRD analyses were also conducted on coated samples after different durations of oxidation for the two temperatures, 750 and 900 °C. At 750 °C, the XRD patterns of Figure 4c show an improved crystallization (or an increased grain density) of the rutile with an increasing duration of oxidation, up to 9 h. At 900 °C, the (211) peak related to TiO_2 appears after 1 min with an intensity higher than that of the (101) peak. Its intensity does not change for longer durations, whereas the intensity of the rutile (101) peak increases up to 1 h and stabilizes for longer durations (Figure 4d).

The D-SIMS depth profiles of samples oxidized from 700 to 950 °C were also realized to correlate the results of the oxidation kinetics to the XRD study with chemical data on the different oxide layers. The depth profiles presented in Figures 5−7 focus on the oxidized part of the coating.

The D-SIMS profiles highlight the formation of a single oxide layer at 700 °C and a multilayer oxide at higher temperatures. At 700 °C, a mixed oxide scale containing all the metallic elements (Ti, Al, and Ta) of the nitride coating develops on the coating for all the durations studied (from 1 to 15 h) as shown in panels a and b of Figure 5. No preferential metallic diffusion is observed. From 750 °C, an Al-rich oxide layer is detected on top of the AlTiTa-mixed oxide layer even for oxidation times as short as 1 h (Figure 6a). With a further increase in the duration of heating (9 h) at 750 °C (Figure 6b) or for temperature up to 800 °C (Figure 6c), the development of an Al-depleted region at the oxide−nitride interface can be detected.

In the range of 850−950 °C, a pure alumina layer could be observed with an extremely low Ti content (<1 atom %) in this layer and the region closer to the oxide−nitride interface is more significantly Al-depleted (Figure 6d−f). The development of this alumina layer is slow at 850 °C (Figure 6d) and becomes faster at 900 °C (Figure 6e), where the alumina layer and the Al-depleted region are already present after oxidation for 1 min (Figure 7). When the temperature is increased from 900 to 950 °C (Figure 6e,f), the alumina layer becomes thicker. This is supported by an increase in sputtering time necessary to go through the Al oxide layer after oxidation for 1 h [from 1886 s at 900 °C to 4474 s at 950 °C (Figure 8)].

Using the sputtering time needed to analyze individual oxides formed at temperatures (750−950 °C) at which an oxide bilayer was developed using D-SIMS, it was possible to estimate the evolution of the thickness of individual oxide components, i.e., alumina and AlTiTa oxide, along with total oxide thickness. The estimation was made on the basis of an underlying assumption that both types of oxides formed have

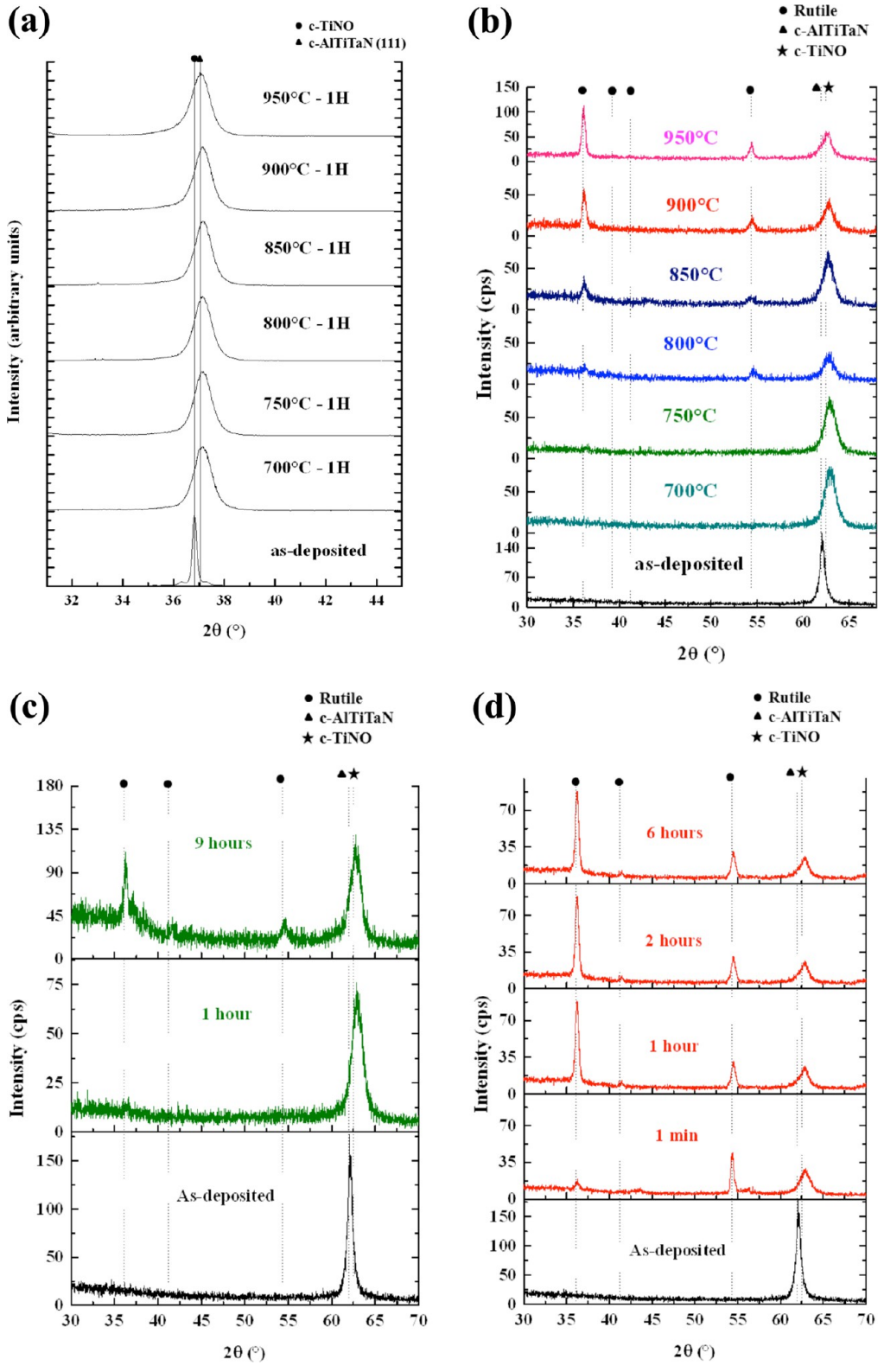

Figure 4. (a) $\theta - 2\theta$ BB XRD spectra and (b) GI XRD spectra for AlTiTaN coatings annealed in air for 1 h at different temperatures from 700 to 950 °C. (c and d) GI XRD spectra for AlTiTaN coatings annealed in air for various durations at 750 and 900 °C, respectively (JCPDS Files 04-001-9292 and 00-021-1276 used for TiNO and rutile, respectively).

uniform an elemental composition throughout. We observed that the evolution of the Al rich layer and the AlTiTa oxide layer and the total oxide thickness followed the same trend with temperature while time was kept constant as shown in Figure 8. This showed that the increase in the oxide thickness above 850 °C is due to an increase in both rates of inward diffusion of O and outward diffusion of Al. It is also interesting to note, on Figure 9b, for long oxidation times at the highest temperatures that Ti starts to outwardly diffuse. This is supported by the presence of Ti in the alumina layer and the

dx.doi.org/10.1021/am405727p | ACS Appl. Mater. Interfaces 2014, 6, 4115−4125

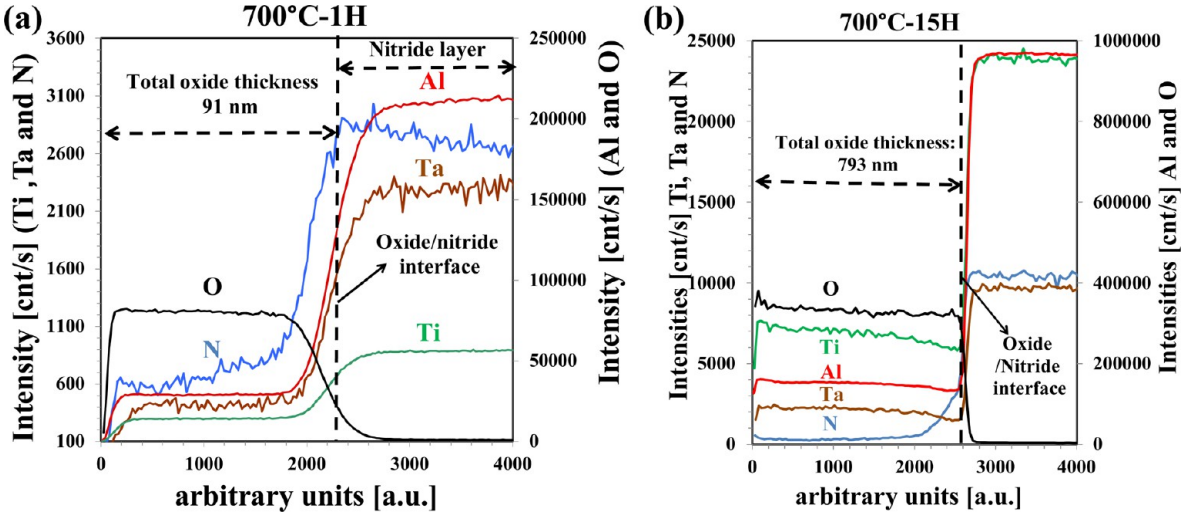

Figure 5. O, Al, Ta, N, and Ti D-SIMS depth profiles for AlTiTaN coatings (oxide layer) oxidized for (a) 1 h and (b) 15 h at 700 °C.

detection of a minor quantity of Ti (0.5 ± 0.4 atom %) via TEM-EDX analysis (Table 2).

4. DISCUSSION

Depending on the temperature of oxidation, two types of oxidation mechanisms can be distinguished in AlTiTaN coatings, the first one in action at 700 °C and the second one in action above 750 °C.

At 700 °C and for all the durations tested, SIMS depth profiles indicate a uniform distribution of the metallic elements in the oxide layer. In the case of a long duration oxidation at 700 °C for 15 h in Figure 5b, an oxy−nitride sublayer could be observed between the oxide and nitride layer, indicating incomplete oxidation of this zone. This suggests that only O has diffused inward and replaced nitrogen in the coating, and this mechanism is in good agreement with those described in other works. According to the works of Endrino et al.[19] on TiAlN and Milosev et al.[20] on TiN, the nitrogen is lost as gaseous N_2 during the oxidation of metallic nitrides. This oxidation mechanism can be considered valid even if Ta is introduced into the nitride coating. As no peak is detected in the XRD pattern, it can be suggested that this mixed oxide is amorphous at this temperature. The amorphous state of this mixed oxide has not, to the best of our knowledge, been reported before this work regarding TiAlN- or AlTiTaN-based coatings. However, Abadias et al.[21] reported the formation of an amorphous oxide in $Ti_{0.7}Ta_{0.3}N$ coatings oxidized at 650 °C.

Several studies present in the literature can help us to explain the presence of this mixed amorphous oxide. Omari et al.[22] have demonstrated that rutile is crystallized very slowly at 700 °C when the TiN coating is oxidized in air for 6 h, but this does not completely support our observation. Hence, observations on other elements present in the matrix, i.e., Al and Ta, that are also oxidized need to be evaluated. Joshi et al.[10] detected the presence of a mixed Ti and Al oxide in TiAlN coatings oxidized at ≤700 °C using Auger electron spectroscopy. However, no crystallographic investigations were performed to determine whether this mixed oxide was crystalline or amorphous.

The kinetic study can conclude that the oxidation rate, which is governed by the inward diffusion of oxygen, is relatively high for this low oxidation temperature. This high oxidation rate could be explained by a grain boundary diffusion mechanism for oxygen. This diffusion mechanism can be supported by the columnar structure of the PVD nitride layer or/and is confirmed by the XRD peak shift to higher angles after annealing corresponding to the presence of the fcc AlTiTaNO (111) phase (Figure 4a).

Oxidation at ≥750 °C results in the formation of an aluminum rich oxide at the top of AlTiTa oxide, and this oxide layer continues to grow with time. The mixed AlTiTa oxide at the interface with the unoxidized part of the nitride coating also grows during the oxidation of the AlTiTaN coatings.

The SIMS profiles show that this mixed Ti/Ta oxide layer also contains Al, but its Al content changes with time. The aluminum depletion zone has been clearly detected by SIMS, and this analysis has shown that the thickness of this area increases with temperature and time. After oxidation at 900 °C for 6 h, this TiTa oxide layer with the low Al concentration constitutes the large part of this mixed oxide (Figure 9b). This layout has been clearly verified after cross-section preparation of a sample oxidized at 900 °C for 6 h and realization of TEM observations (Figure 9a). Both techniques, i.e., BFTEM (Figure 9a) and dynamic SIMS (Figure 9b), clearly demonstrated the presence of alumina- and titanium-based oxide containing both Al and Ta. A clearer picture could be obtained through the HAADF (high-angle annular dark field) TEM image of this sample as displayed in Figure 10. The titanium-based oxide layer presents a gradient of Al composition that increases with time. It can be proposed that the Al depletion of the titanium-based oxide layer with time follows with crystallization of the titanium-based oxide as the rutile phase. The presence of an alumina layer (Al_2O_3) on top was confirmed by TEM and EDX, and the results of the quantitative estimation of these elements in this layer are listed in Table 2. Ta and Ti (for <900 °C) are relatively immobile, as revealed by the sharp interface between alumina and the AlTiTa mixed oxide layer in the SIMS depth profile of Figure 10b and by the complete absence of this element in the alumina layer revealed by TEM and EDX as shown in Table 2. It must be pointed out that the TEM−EDX measurement gives an oxygen concentration in the range of 51−53 atom % in the AlTiTa oxide layer containing rutile crystallites. This content of oxygen is far below the stoichiometry of the rutile TiO_2 phase (66 atom %), which should be ideally observed. This irregularity can be explained by three factors: (a) an instrumental error as the EDX measurement is taken through a volume that is larger than the volume of crystallites, (b) an incorporation of atomic oxygen at the grain boundaries, and (c) the presence of amorphous oxide under stoichiometric conditions in O.

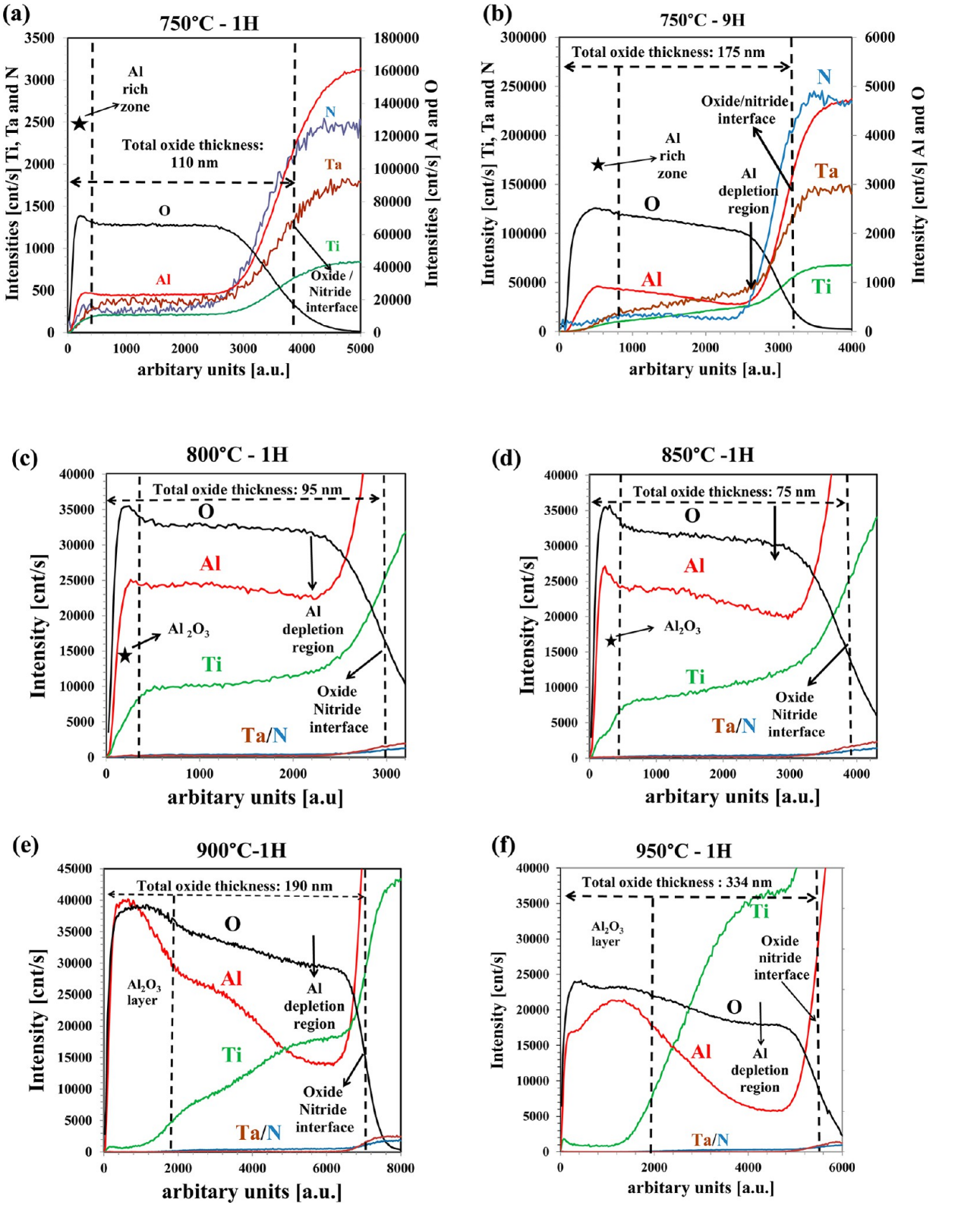

Figure 6. O, Al, Ti, Ta, and N D-SIMS depth profiles for AlTiTaN coatings (oxide layer only) oxidized for 1 h at (a) 750, (c) 800, (d) 850, (e) 900, and (f) 950 °C and (b) for 9 h at 750 °C. Note that the oxygen intensity has been halved for better visualization of the data.

The structural evaluation of the oxide layer improves our understanding of the change in the oxidation mechanism. As the GI XRD analysis (Figure 4b–d) shows that the intensity of the rutile peak increases with temperature and exposure time, it can be proposed that the aluminum depletion process follows the crystallization of the AlTiTa oxide into the rutile phase. This final formation of the bilayer oxide at ≥750 °C can be possible if two diffusion processes can be activated: inward diffusion of oxygen until the nitride–oxide interface and outward diffusion of aluminum from the AlTiTa mixture oxide. The higher mobility of

dx.doi.org/10.1021/am405727p | ACS Appl. Mater. Interfaces 2014, 6, 4115–4125

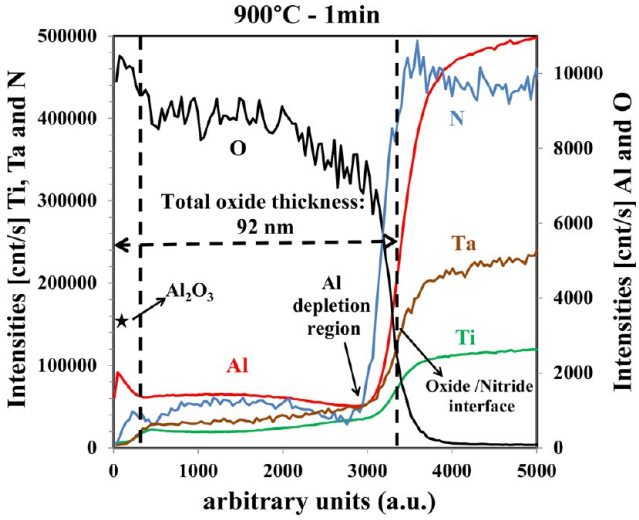

Figure 7. D-SIMS depth profiles in the oxide layer of an AlTiTaN coating oxidized for 1 min at 900 °C.

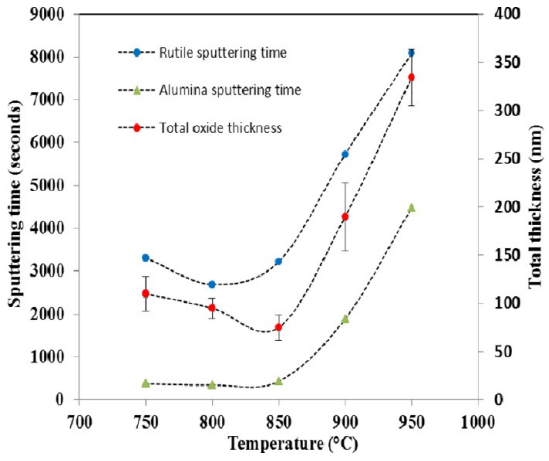

Figure 8. Comparison of SIMS sputtering times necessary to cross the whole alumina layer (circles) and the whole "rutile" layer (squares) and the evolution of the total oxide layer (triangles) formed after 1 h for the different temperatures studied.

Table 2. TEM−EDX Atomic Compositions of the Oxide Layer Developed on the AlTiTaN Coating Air-Annealed at 900 °C for 6 h

	concentration (atom %)		
element or zone	alumina layer	Al rich AlTiTa oxide layer	TiTa rich AlTiTa oxide layer
O	57 ± 5	53 ± 5	51 ± 5
Al	42.5 ± 3	28 ± 2	9 ± 1
Ti	0.5 ± 0.4	13 ± 1	27 ± 1
Ta	0	6 ± 1	13 ± 1

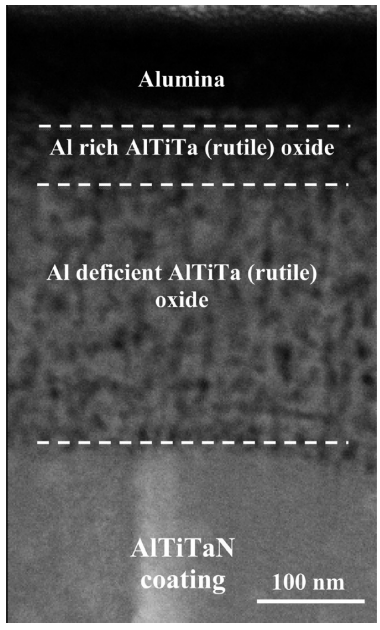

Figure 10. HAADF−STEM image showing the presence of amorphous alumina (dark contrast) in the rutile layer.

metallic ions like Al (0.5 Å) and gaseous O compared to those of larger ions like Ti^{4+} (0.61 Å) and Ta^{5+} (0.65 Å) in the range of 750−900 °C has been described previously.[2] McIntyre et al.[2] reported that these two light elements were

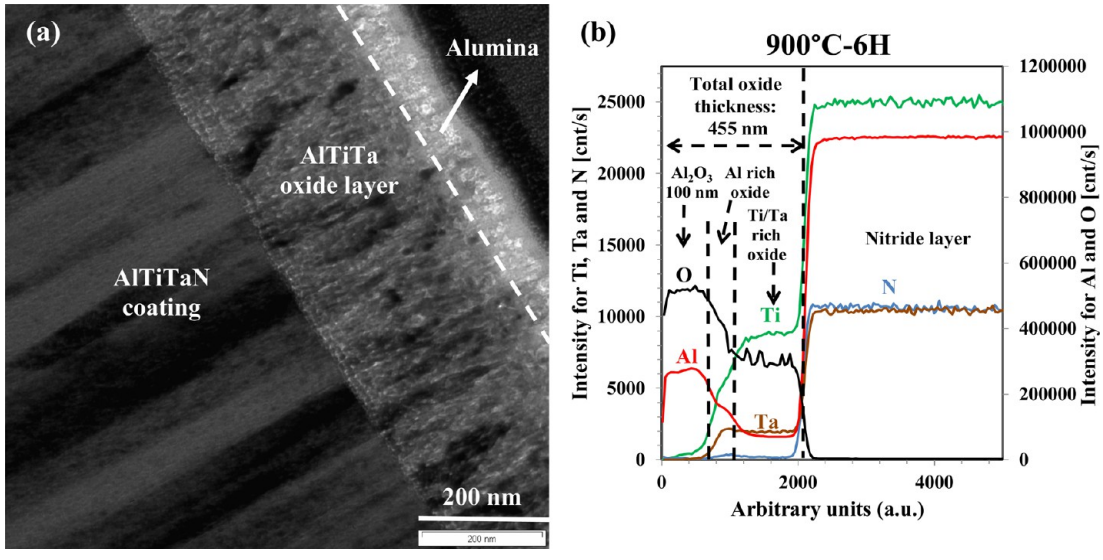

Figure 9. AlTiTaN coating air-annealed at 900 °C for 6 h: (a) bright field TEM (BF-TEM) image and (b) D-SIMS depth profile.

dx.doi.org/10.1021/am405727p | ACS Appl. Mater. Interfaces 2014, 6, 4115−4125

the more mobile species during the oxidation of TiAlN coatings at 750 °C.

Crystallization of the rutile phase could be the process that initiates the outward diffusion of the aluminum at 750 °C as it is known that the solubility of Al in the rutile phase is low.[23] The formation of new grain boundaries richer in defects would result in better pathways for the outward diffusion of Al at ≥750 °C. Yan et al.[24] showed that small cations (0.5 Å) like Al^{3+} can easily diffuse through interstitial sites within the rutile matrix. Hence, from the crystalline rutile lattice (AlTiTa oxide), Al diffuses more easily out toward the sample surface. This promotes Al diffusion at 750 °C at the surface and preferential formation of alumina at the top surface from 800 °C onward.

The presence of amorphous alumina, instead of the crystallized form, on top of the oxidized coatings in the range of temperatures between 750 and 950 °C has also been indicated in other publications. Chaudhuri et al.[25] reported in a single crystal of AlN oxidized at 800 °C, the formation of amorphous alumina, and they attributed these results to alumina's relatively high Gibbs free energy of formation (−420.7 kcal/mol at 623 °C[26]), which inhibits its crystallization.

The formation of a very thin alumina layer could further provide additional oxidation resistance. At this stage, it could be possible to propose that the oxidation behavior of these coatings is primarily controlled by the rutile-containing layer (for an air annealing duration of 1 h). Consequently, with time, the free aluminum atoms from the rutile phase area, which outwardly diffuse and react with O to form the alumina top layer, should efficiently decrease the oxidation rate. However, as this very thin aluminum oxide top layer is still amorphous and has an unknown density, it is difficult to evaluate its effective diffusion barrier capabilities during oxidation. Moreover, for longer durations (≥6 h) and higher temperatures (≥900 °C), a preferential outward diffusion of Ti compared with Ta is observed in the D-SIMS profile (Figure 9b).

With regard to the rutile oxide layer, Guidi et al.[18] also showed that the presence of Ta reduces the coalescence of the grains in nanostructured TiO_2 at <850 °C. Compared to the literature, it was demonstrated by McIntyre et al.[2] that this change from a slow oxidation rate to a fast oxidation rate takes place from 800 °C onward for TiAlN coatings. There is an increase in this switching temperature from 800 to 850 °C due to the addition of tantalum to AlTiN coatings. Ta reduces oxygen vacancies in the rutile lattice, which assists in reducing the rate of inward diffusion of oxygen. However, beyond this temperature, i.e., 900 °C, thermal energy is sufficient to overcome this resistance to oxygen inward diffusion and/or decomposition of c-TiTaN and c-AlN phases occurs, leading to the fast oxidation of the AlTiTaN coatings under investigation.

The total oxide thickness is quite stable from 750 to 850 °C (~100 nm) because of the slow crystallization of rutile in this temperature range as shown in Figure 8. Because the volume of rutile is small, the number of pathways for the easy inward diffusion of oxygen is reduced. However, beyond 850 °C, the thickness of the oxide starts increasing rapidly with temperature, keeping the duration of air annealing constant (Figure 8). In addition to a higher mobility of atoms due to the higher temperature, two parallel processes are responsible for this huge increase in the oxidation rate at 900 °C. First, at ≥900 °C, a significant aluminum depletion region at the interface with the nitride layer is formed (Figure 6), leading to a more defective oxide layer and an increase in the rates of inward diffusion of O and outward diffusion of Al. Second, the appearance of the decomposition of AlTiTaN into c-TiTaN and c-AlN phases may start to decrease the diffusion barrier properties of rutile formed. These processes result in the formation of different oxide layers with lower diffusion barrier capabilities.

Pfeiler et al.[6] showed that the AlTiTa mixed oxide layer in their samples oxidized at 900 °C for 5 h consists of a TiTa rich layer that is a porous layer at the nitride interface and a dense rutile layer containing Al and Ta at the alumina−AlTiTa oxide interface. No such porosity could be observed in the coating investigated here. One possible reason for this is the larger amount of Al (28 atom %) for coatings evaluated by Pfeiler et al.[6] compared to 22 atom % Al in the AlTiTaN coating investigated here. The high Al concentration gradient of Al observed by Pfeiler et al.[6] leads to greater outward diffusion of Al (alumina:AlTiTa oxide thickness ratio of ~50:50) and void formation. This leads to an alumina comparatively thicker than that observed in our case (alumina:AlTiTa oxide thickness ratio of ~25:75), but the porosity generated in the AlTiTa oxide layer may be detrimental to coating adhesion. For this reason, a lower content of Al is more appropriate for these kinds of coatings.

The effect of Ta in AlTiTaN coatings on the temperature up to which an amorphous oxide is possible can also be considered. McIntyre et al.[2] investigated the air oxidation of TiAlN coatings from 750 °C onward and observed crystalline oxide formation at this temperature. Comparing these results to those obtained in this work, we found addition of Ta does not influence the critical temperature needed for the formation of amorphous or crystalline oxide compared to that of AlTiN. For confirmation, further study of this aspect of the AlTiTaN coating is needed.

A scheme summarizing the different types of oxides resulting from air annealing of AlTiTaN coatings in the temperature range of 700−950 °C is illustrated in Figure 11. Three kinds of oxides

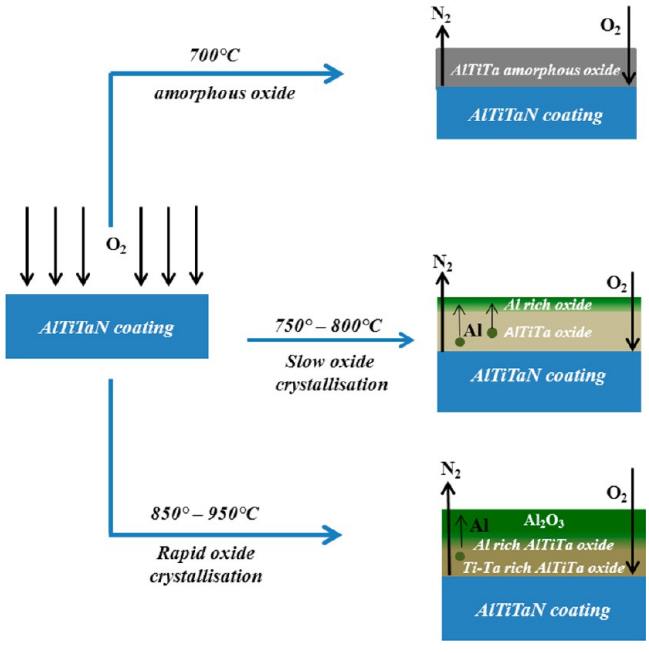

Figure 11. Schematic representation of the different types of oxides formed on AlTiTaN coatings when they are air annealed in the temperature range of 700−950 °C. The evolution from the amorphous oxide layer to the crystalline oxide layer is represented by the dark to light contrast in the AlTiTa oxide layer.

dx.doi.org/10.1021/am405727p | ACS Appl. Mater. Interfaces 2014, 6, 4115−4125

were observed depending on the air oxidation temperature. At 700 °C, an amorphous AlTiTa oxide is observed. Within the temperature range of 750−850 °C, an AlTiTa oxide with crystalline rutile grains is formed with an Al rich top layer facilitated by outward diffusion of Al. At temperatures from 850 to 950 °C, the process of crystallization is fast and two different types of AlTiTa oxide layers can be observed (Al rich and TiTa rich) along with a pure alumina layer on top of the AlTiTa oxide layer.

5. CONCLUSIONS

Oxidation resistant AlTiTaN coatings deposited at 265 °C with a fiber (111) texture have been elaborated using DC magnetron sputtering technique. An enhanced thermal stability of the AlTiTaN coating could be observed compared to those of TiAlN coatings found in the literature. With respect to the oxidation mechanism, oxidation in $Al_{0.48}Ti_{0.40}Ta_{0.12}N$ coatings is primarily controlled by the inward diffusion of oxygen and/or outward diffusion of Al. Depending on the oxidation temperature, one of the diffusion processes predominates. At 700 °C, only inward diffusion of oxygen leads to a relatively high oxidation rate of the coating for all oxidation durations. At ≥750 °C, both inward diffusion of oxygen and outward diffusion of Al take place, leading to an oxide bilayer and with time to crystallization of the AlTiTa mixed oxide. Because of the outward diffusion of Al, the formation of an alumina top layer provides the necessary resistance to further oxidation at 900 °C. In both cases, parabolic oxide layer growth is observed, but the lower slope at 900 °C provides oxidation resistance to the coating that is better than that at 700 °C. No porosity is formed on the inner side of the oxide layer as observed in other works due to the smaller amount of Al in the coatings. In conclusion, the Al:Ti ratio selected here and the addition of Ta seem to be a good compromise, with the deposition conditions, for producing high-temperature oxidation resistant coatings. To further increase the oxidation resistance, higher deposition temperatures and addition of a fifth element are under investigation.

AUTHOR INFORMATION

Corresponding Author

*E-mail: duday@lippmann.lu.

Notes

The authors declare no competing financial interest.

ACKNOWLEDGMENTS

The financial support by the National Research Fund (FNR, Luxembourg) under the frame of the SpiTriCoat project is gratefully acknowledged. Valuable time provided by Dr. B. Girault for the optimization of our in-house DC magnetron sputtering system and support for XRD investigations and Dr. A. Botor-Probierz for TEM investigations and support provided by B. El Adib for making D-SIMS characterisations are gratefully acknowledged. Useful suggestions provided by Dr. Remi Aninat and Dr. Jérôme Guillot are also appreciated.

REFERENCES

(1) Hörling, A.; Hultman, L.; Odén, M.; Sjölén, J.; Karlsson, L. Mechanical properties and machining performance of Ti1-xAlxN-coated cutting tools. *Surf. Coat. Technol.* **2005**, *191*, 384−392.

(2) McIntyre, D.; Greene, J. E.; Hakansson, G.; Sundgren, J.-E.; Münz, W.-D. Oxidation of metastable single-phase polycrystalline $Ti_{0.5}Al_{0.5}N$ films: Kinetics and mechanisms. *J. Appl. Phys.* **1990**, *67*, 1542−1553.

(3) Veprek, S.; Haussmann, M.; Reiprich, S.; Li, S.; Dian, J. Novel thermodynamically stable and oxidation resistant superhard coating materials. *Surf. Coat. Technol.* **1996**, *86*−*87*, 394−401.

(4) Barshilia, H. C.; Ghosh, M.; Ramakrishna, S. R.; Rajam, K. S. Deposition and characterization of TiAlSiN nanocomposite coatings prepared by reactive pulsed direct current unbalanced magnetron sputtering. *Appl. Surf. Sci.* **2010**, *256*, 6420−6426.

(5) Kathrein, M.; Michotte, C.; Polick, P. Coated tool. U.S. Patent 7,521,132 B2, April 21, 2009.

(6) Pfeiler, M.; Scheu, C.; Hutter, H.; Schnöller, J.; Michotte, C.; Mitterer, C.; Kathrein, M. On the effect of Ta on improved oxidation resistance of Ti−Al−Ta−N coatings. *J. Vac. Sci. Technol., A* **2009**, *27*, 554−560.

(7) Pfeiler, M.; Fontalvo, G. A.; Wagner, J.; Kutschej, K.; Penoy, M.; Michotte, C.; Mitterer, C.; Kathrein, M. Arc Evaporation of Ti-Al-Ta-N Coatings: The Effect of Bias Voltage and Ta on High-temperature Tribological Properties. *Tribol. Lett.* **2008**, *30*, 91−97.

(8) Rachbauer, R.; Holec, D.; Mayrhofer, P. H. Increased thermal stability of TiAlN thin films by Ta alloying. *Surf. Coat. Technol.* **2012**, *211*, 98−103.

(9) Ichimura, H.; Kawana, A. High-temperature oxidation of ion-plated TiN and TiAlN films. *J. Mater. Res.* **1993**, *8*, 1093−1100.

(10) Joshi, A.; Hu, H. S. Oxidation behavior of titanium-aluminium nitrides. *Surf. Coat. Technol.* **1995**, *76*−*77* (2), 499−507.

(11) Mezin, A. Coating internal stress measurement through the curvature method: A geometry-based criterion delimiting the relevance of Stoney's formula. *Surf. Coat. Technol.* **2006**, *200*, 5259−5267.

(12) Sangiovanni, D. G.; Chirita, V.; Hultman, L. Toughness enhancement in TiAlN-based quarternary alloys. *Thin Solid Films* **2012**, *520*, 4080−4088.

(13) Mukherjee, S.; Gall, D. Structure zone model for extreme shadowing conditions. *Thin Solid Films* **2013**, *527*, 158−163.

(14) Fullerton, E. E.; Schuller, I. K.; Vanderstraeten, H.; Bruynseraede, Y. Structural refinement of superlattices from X-ray diffraction. *Phys. Rev. B* **1992**, *45* (16), 9292−9310.

(15) Abadias, G.; Leroy, W. P.; Mahieu, S.; Depla, D. Influence of particle and energy flux on stress and texture development in magnetron sputtered TiN films. *J. Phys. D: Appl. Phys.* **2013**, *46*, 055301-9.

(16) Holec, D.; Zhou, L.; Rachbauer, R.; Mayrhofer, P. H. Alloying-related trends from first principles: An application to the Ti−Al−X−N system. *J. Appl. Phys.* **2013**, *113*, 113510-8.

(17) Guidi, V.; Carotta, M. C.; Ferroni, M.; Martinelli, G.; Sacerdoti, M. Effect of Dopants on Grain Coalescence and Oxygen Mobility in Nanostructured Titania Anatase and Rutile. *J. Phys. Chem. B* **2003**, *107*, 120−124.

(18) Reddy, R. G.; Li, Y.; Arenas, M. F. Oxidation of a Ternary Ti_3Al-Ta Alloy. *High Temp. Mater. Processes (Berlin, Ger.)* **2002**, *21*, 195−205.

(19) Endrino, J. L.; Arhammar, C.; Gutirrez, A.; Gago, R.; Horwat, D.; Soriano, L.; Fox-Rabinovich, G.; Marero, D.; Guo, J.; Rubensson, J. E.; Andersson, J. Spectral evidence of spinodal decomposition, phase transformation and molecular nitrogen formation in supersaturated TiAlN films upon annealing. *Acta Mater.* **2011**, *59*, 6287−6296.

(20) Milosev, I.; Strehblow, H.-H.; Navingek, B. XPS in the study of high-temperature oxidation of CrN and TiN hard coatings. *Surf. Coat. Technol.* **1995**, *74*−*75*, 897−902.

(21) Abadias, G.; Koutsokeras, L. E.; Siozios, A.; Patsalas, P. Stress, phase stability and oxidation resistance of ternary Ti-Me-N (Me = Zr, Ta) hard coatings. *Thin Solid Films* **2013**, *538*, 56−70.

(22) Omari, M. A.; Sorbello, R. S.; Aita, C. R. Crystallization and segregation in vitreous rutile films annealed at high temperature. *J. Vac. Sci. Technol., A* **2005**, *23*, 1568−1574.

(23) Slepetys, R. A.; Vaughan, P. A. Solid solution of aluminium oxide in rutile titanium dioxide. *J. Phys. Chem.* **1969**, *73*, 2157−2162.

(24) Yan, M. F.; Rhodes, W. W. Effects of cation contaminants in conductive TiO_2 ceramics. *J. Appl. Phys.* **1982**, *53*, 8809−8818.

(25) Chaudhuri, J.; Nyakiti, L.; Lee, R. G.; Gu, Z.; Edgar, J. H.; Wen, J. G. Thermal oxidation of single crystalline aluminum nitride. *Mater. Charact.* **2007**, *58*, 672.
(26) Bhansali, A. S.; Sinclair, R.; Morgan, A. E. A thermodynamic approach for interpreting metallization layer stability and thin-film reactions involving four elements: Application to integrated circuit contact metallurgy. *J. Appl. Phys.* **1990**, *68*, 1043.